E. Salahinejad, R. Amini, E. Askari Bajestani, M. Hadianfard, *Microstructural and hardness evolution of mechanically alloyed Fe–Cr–Mn–N powders*, Journal of alloys and compounds, 497 (2010) 369-372.
https://doi.org/10.1016/j.jallcom.2010.03.071

# Microstructural and hardness evolution of mechanically alloyed Fe–Cr–Mn–N powders

E. Salahinejad [a,*], R. Amini [b], E. Askari Bajestani [a], M. J. Hadianfard [a]

[a] Department of Materials Science and Engineering, School of Engineering, Shiraz University, Zand Blvd., 7134851154, Shiraz, Iran

[b] Department of Materials Science and Engineering, Shiraz University of Technology, Modarres Blvd., 3619995161, Shiraz, Iran

## Abstract

The effect of milling time on the structure and hardness of Fe–18Cr–4Mn–$x$N alloy powders processed by mechanical alloying is investigated. According to X-ray diffraction and transmission electron microscopy evaluations, complete amorphization is achieved beyond 126 h of milling. That is, the powders milled for the shorter durations are nanocrystal dispersed amorphous matrix composites. Microindentations on the as-milled powders reveal that the hardness of the nanocomposites first increases and then decreases by the amorphization progression. However, the hardness of the fully amorphous alloys progressively decreases by increasing the milling time.

**Keywords:** Nanostructured material; Amorphous materials; Mechanical alloying; Mechanical properties; Microstructure; Transmission electron microscopy

---

[*] **Corresponding Author:** *Email address:* erfan.salahinejad@gmail.com (Erfan Salahinejad)

**This is the accepted manuscript (postprint) of the following article:**
E. Salahinejad, R. Amini, E. Askari Bajestani, M. Hadianfard, *Microstructural and hardness evolution of mechanically alloyed Fe–Cr–Mn–N powders*, Journal of alloys and compounds, 497 (2010) 369-372.
https://doi.org/10.1016/j.jallcom.2010.03.071

## 1. Introduction

Mechanical alloying (MA) is a versatile solid-state method to synthesize a wide variety of equilibrium and non-equilibrium structures, including supersaturated, metastable crystalline, quasicrystalline, intermetallic, nanostructured, and amorphous alloys [1,2]. Milling time is one of the most important variables of MA that considerably affects contamination, structure, and properties of the product. Because of this, this is one of the most frequently studied topics in the field of MA for various alloys, for instance Refs. [3–6].

Generally, milling is conducted under an inert gas like argon or helium to prevent undesirable oxidation and contamination. Nonetheless, milling of reactive powders such as titanium, aluminum, iron, and their alloys in the presence of a nitrogen ambience introduces nitrogen into the matrix via a solid–gas reaction. Thus, to develop nickel-free high-nitrogen stainless steels (particularly Fe–Cr–Mn–N alloys), it has been of interest to study MA of these alloys under a nitrogen atmosphere allowing the incorporation of nitrogen into the matrix. It would be worth mentioning that in these alloys, manganese is added to increase the solubility of nitrogen [7].

In recent years, noticeable researches on MA of stainless steels under a nitrogen atmosphere have been reported [8–18]. It has been recognized that nitrogen has a key contribution to amorphization in this alloy system. In addition, aspects of phase transformations occurring during MA, thermal behavior, and magnetic properties of the Fe–Cr–Mn–N powders have been evaluated [8–11]. However, it seems that further researches are required to be conducted on other properties, particularly on their mechanical properties. To the best of our knowledge, little systematic work has been reported on mechanical properties of nanocrystalline/amorphous and fully amorphous stainless steels. In this work, stainless steel powders with compositions of Fe–18Cr–4Mn–$x$N were synthesized by MA under a

E. Salahinejad, R. Amini, E. Askari Bajestani, M. Hadianfard, *Microstructural and hardness evolution of mechanically alloyed Fe–Cr–Mn–N powders*, Journal of alloys and compounds, 497 (2010) 369-372.
https://doi.org/10.1016/j.jallcom.2010.03.071

nitrogen atmosphere. The effect of milling time on the microhardness of the as-milled powders is considered via evaluating their microstructures by X-ray diffraction (XRD) and transmission electron microscopy (TEM).

## 2. Experimental procedure

Fe (>99.5%, $D_{av.}$ = 50 μm), Cr (>99.9%, $D_{av.}$ = 150 μm), and Mn (>99.9%, $D_{av.}$ = 50 μm) powders supplied by Merck with a nominal composition of 78Fe–18Cr–4Mn (wt.%) were milled in a planetary ball mill (Fritsch, Pulverisette 5). Milling was conducted in a sealed container with a capacity of 250 mL that had been filled with pure nitrogen gas. A rotation speed of 250 rpm and a ball-to-powder weight ratio of 30:1 were employed. Powder sampling was performed at 9-h intervals, ranging from 99 h to 153 h, inside a nitrogen glove box.

To assess powder contamination introduced during MA, elemental analyses were accomplished by a LECO gas analyzer (Corp., St. Joseph, MI) and X-ray fluorescence analyzer (XRF, Philips PW2400). The phase analysis of the as-milled powders was carried out by XRD (Shimadzu Lab X-6000 with Cu Kα radiation). The XRD experiments were quantitatively analyzed by TOPAS 3 from Bruker AXS. The relative content of present phases was estimated by the Rietveld method and the average crystallite size of crystalline phases was determined by the Double-Voigt approach. Note that the amorphous phase amounts were also estimated by Rietveld analyzing the XRD data. The validity of the XRD results was checked by TEM (JEOL-JEM 2010). The TEM powder samples were prepared by dispersing the powder particles in ethanol and dropping down them in a copper rigid.

For microhardness measurements, the surface of compacts obtained from the as-milled powders was polished. Then, the cross section of the powder particles was indented under a

25 g load and a 15 s dwell time at room temperature. To have accurate results, at least five indents were conducted on each sample and subsequently averaged.

## 3. Results and discussion

Table 1 lists the results of the elemental analyses conducted by LECO and XRF. It is noticeable that the anticipated nominal composition (18Cr–4Mn) has been obtained and the only detectable impurity has been oxygen. This is attributed to the natural oxidation of the powders in the atmosphere, which is insignificant and the same for all the samples. It is seen that the nitrogen content increases with milling time due to a solid-gas reaction, approaching 3.76 wt.% after 153 h of milling. Since the powder particles are subjected continual fracturing and plastic deformation due to the action of the milling media, fresh surfaces are created. These virgin surfaces are very prone to react with any active species presented in the environment. When milling is conducted under nitrogen gas, molecular nitrogen adheres on the newly exposed surfaces, dissociates, and consequently penetrates into the matrix via cold welding of the particles and diffusing down to interstitial sites, grain boundaries, dislocations, and other defects. It is believed that the chemisorption of nitrogen onto the clean surfaces created by milling is the essential step governing the solid–gas reaction [19,20].

Table 1

Fig. 1 demonstrates the XRD traces of the initial powder mixture and the powders milled for 99, 108, 117, 126, 135, 144, and 153 h. The results of the XRD analyses consisting of the relative phase amount and the crystallites size are summarized in Table 2. According to the Rietveld analysis, three different phases, namely ferrite ($\alpha$), austenite ($\gamma$), an amorphous phase, are recognizable. It is seen that the samples milled for 99, 108, and 117 h exhibit a nanocomposite structure consisting of the amorphous phase plus the nanocrystals. In contrast, the powders milled for the times more than 126 h possess a single amorphous structure. Details of the calculations related to the amorphous quantitative analysis by the Rietveld method have been illustrated in Ref. [8]. It is noted that since the present research aims to focus on the nitride-free alloys, nitride-containing samples milled for the longer times are not considered here. This is the cause of selecting 152 h as the maximum milling time studied.

Fig. 1

Table 2

To evaluate the validity of the XRD results, TEM studies were conducted on the powders. Typically, Fig. 2 represents the TEM micrograph of the powders milled for 117 and 126 h having the nanocomposite and amorphous structures respectively, in accordance with the XRD analyses. The selected area diffraction (SAD) patterns related to the sample milled for 117 h imply that the dark regions are a combination of the nanocrystalline $\alpha$- and $\gamma$-phases and the bright matrix is a featureless amorphous phase (Fig. 2a). On the contrary, the TEM micrograph of the sample milled for 126 h exhibits no contrast and the corresponding SAD pattern represents a homogenous hallo pattern attributed to a fully amorphous structure (Fig. 2b). No diffraction spots or sharp diffraction rings related to crystalline phases can be detectable and merely diffraction hallos associated with the amorphous phase can be observed. The insignificant amount of oxygen in the sample (Table 1) suggests that the single-phase amorphous structure cannot be oxide. That is, the TEM assessments confirm what the XRD analyses provided already. Thus, two major microstructural evolutions were detected during MA of the powder: nanograin refinement and amorphization.

Fig. 2

Concerning MA of stainless steels under a nitrogen atmosphere, it has been reported that the $\gamma$-grain size reaches about 7 nm after 60 h [15], 6 nm after 120 h [13], 5 nm after 144 h [8], and 3.3 nm after 170 h of milling [12], which is comparable with the results of this study. During MA, the powder particles are subjected to severe plastic deformation, thereby increasing the density of dislocations and developing shear bands containing high dislocation densities. Afterwards, dislocation cells and subgrains separated by low-angle grain boundaries are formed to decrease lattice strain. Consequently, the transformation of the low-angle to high-angle grain boundaries takes place by grain rotation, giving nanostructures [1]. It has been also realized that the incorporation of nitrogen during MA is another source for the grain refinement [8]. Diffused nitrogen atoms are segregated at dislocations and grain boundaries, fixing the dislocations and stabilizing the grain boundaries. Afterward, the trickling down of mobile dislocations on the fixed dislocations contributes to the nucleation of new boundaries and severe grain refinement [21]. It is worthwhile to note nitrogen enhances the self-diffusion activation energy and hardness, in contrast, reduces the stacking fault energy and shear modulus in the Fe–Cr–Mn–N alloys [8], thereby intensifying the structural refinement based on the dislocation-based model proposed by Mohammad [22] estimating the minimum grain size achievable by MA.

Regarding amorphization, the results presented above suggest that by increasing the milling time, the amorphous phase content increases; and amorphization is completed beyond

126 h of milling. The amorphization reaction can be argued in terms of the high energy given to the powders during milling and the contribution of nitrogen. The extreme structural refinement that has occurred during milling increases the constraints of the neighboring crystallites, decreasing the stability of the crystalline structure. Moreover, nitrogen intensifies the structural refinement aiding amorphization. On the other hand, nitrogen in the Fe–Cr–Mn–N alloys increases the atomic size mismatch and negative heat of mixing among the constituent elements [8], encouraging amorphization significantly according to the Inoue's empirical rules [23]. Note that since the amorphous phase nucleates at grain boundaries and grows by interdiffusion reaction [14], the nanocrystalline phase dispersed amorphous matrix composites are developed during MA.

The microhardness results of the as-milled powders are signified in Fig. 3, implying significant hardnesses attributed to the strong bonding between the constituent elements. Since the indentations were done on pore-free zones of the compacts and since the ratio of the indent-to-powder particle size was sufficiently small, the effect of pores on the microhardness results can be supposed to be negligible. It is noted that the powders particle size exceeded 10 μm. Considering the microstructure of the powders, let us divide the hardness plot into three parts, namely parts A, B, and C. Part A corresponds to the samples having the composite structure (consisting of the amorphous phase and nanocrystals), where the hardness increases with the milling time. Part B corresponds to the samples milled for 117 and 126 h exhibiting the composite and the fully amorphous structures respectively, in which the hardness decreases with the milling time. Part C corresponds to the fully amorphous samples, where the hardness decreases with the milling time progressively.

Fig. 3

The hardness behavior in part A is attributed to the difference in the amorphous phase content of the powders (Table 2). Since essentially amorphous phases have higher hardness than crystalline structures, it is inferred that this effect governs the hardness trend in this range of milling time up to 117 h. It should be noted that the powders milled for durations less than 99 h showed the similar behavior; therefore, the minimum milling time focused in this paper was 99 h. On the other hand, it is seen that the complete amorphization due to 126 h of milling has gave rise to a sharp drop in hardness from 1120 to 1070 HV for the samples milled for 117 and 126 h respectively (part B). It suggests that although homogeneous amorphous structures exhibit hardnesses more than single crystalline ones, the sample with the amorphous-nanocrystalline composite structure signifies higher hardness than the amorphous material. That is, the behavior of part B contradicts that of part A in which the hardness increases with the amorphous phase content.

The trend in part B is explained in terms of the strengthening effect of precipitation of nanoscale particles into an amorphous matrix. Firstly, the nanoscale particles are too small to contain defects [24]; therefore, these can be assumed perfect crystals with a substantial hardness. Secondly, since the interfacial energy at the amorphous/crystal interface is lower than that at the crystal/crystal interface [25], the resultant dense packed structure suppresses the propagation of shear bands and cracks along these interfaces. Finally, the dispersion of the nanoscale particles could suppress the deformation of the amorphous phase accomplished by shear sliding. These strengthening mechanisms are responsible for the higher hardness of the nanocomposite. Hence, it is deduced that in this range of milling time, the effect of the nanocomposite strengthening prevails over that of the amorphous phase percentage on the hardness behavior.

The decrease in hardness by increasing the milling time in part C is due to the increase in the nitrogen content. This is explained from the points of view of the bonding configuration and electronic structure of the alloys. Owing to strong interatomic interactions between Fe–N, Cr–N, and Mn–N pairs [8,10,11], some electrons of the metallic bonds are transferred to the metal-nitrogen bonding regions. Because of the fact that N atoms possess a higher electronegativity than Fe, Cr, and Mn atoms, a strong accumulation of electrons forms near N atoms. This leads to a depletion of electrons towards Fe, Cr, and Mn atoms, thereby weakening the metallic bonds. As a result, shear bands are able to initiate from these weakened intercluster regions, resulting in a decrease in hardness by increasing the nitrogen concentration [10]. Note that the hardness behavior observed in these amorphous materials is completely in disagreement with the strengthening effect of nitrogen in crystalline Fe-based alloys, due to differences in the related deformation mechanisms. Concerning the effect of nitrogen on the electronic structure of Fe-based alloys, it is noteworthy that electron localizations have been realized in austenitic steels with nitrogen concentrations higher than 0.4 wt.%, i.e. a decrease in the conduction electrons concentration and consequently an increase in the covalent character of the interatomic bonds, inducing clustering [26]. Eventually, it is noted that aspects of sintering and mechanical behaviors of these mechanically alloyed Cr–Mn–N stainless steels have been recently reported [27–29].

## 5. Conclusions

Fe–18Cr–4Mn–$x$N alloy powders were synthesized by MA under a nitrogen gas atmosphere. The effect of milling time on their structure and microhardness was investigated. The following results and conclusions emerge from the present study:

1. The powders milled for the times less than 126 h displayed nanocrystalline-amorphous composite structures. However, the structure was transformed to a homogeneous amorphous one after 126 h of milling.

2. In the samples with the nanocomposite structure, the hardness increased with the milling time to 117 h due to the influence of the amorphous content.

3. The powder milled for 117 h depicted a higher hardness compared to the fully amorphous structures, because of the effect of the nanocomposite strengthening.

4. By increasing the milling time, a decrease in the hardness of the amorphous materials was found. This was attributed to variations in the nature of the atomic bonds among the constituent elements, caused by the increase in the nitrogen concentration.

## References

[1] C. Suryanarayana, Prog. Mater. Sci. 46 (2001) 1-184.

[2] C. Suryanarayana, E. Ivanov, V.V. Boldyrev, Mater. Sci. Eng. A 304-306 (2001) 151-158.

[3] P. Amornpitoksuk, S. Suwanboon, J. Alloys Compd. 462 (2008) 267-270.

[4] H. Zuhailawati, Y. Mahani, J. Alloys Compd. 476 (2009) 142-146.

[5] A. Jain, S. Agarwal, I.P. Jain, J. Alloys Compd. 480 (2009) 325-328.

[6] W. Chaisan, R. Yimnirun, S. Ananta, Ceram. Int. 35 (2009) 173-176.

[7] M. Sumita, T. Hanawa, S.H. Teoh, Mater. Sci. Eng. C 24 (2004) 753-760.

[8] R. Amini, M.J. Hadianfard, E. Salahinejad, M. Marasi, T. Sritharan, J. Mater. Sci. 44 (2009) 136-148.

[9] R. Amini, H. Shokrollahi, E. Salahinejad, M.J. Hadianfard, M. Marasi, T. Sritharan, J. Alloys Compd. 480 (2009) 617-624.

E. Salahinejad, R. Amini, E. Askari Bajestani, M. Hadianfard, *Microstructural and hardness evolution of mechanically alloyed Fe–Cr–Mn–N powders*, Journal of alloys and compounds, 497 (2010) 369-372.
https://doi.org/10.1016/j.jallcom.2010.03.071

[10] E. Salahinejad, R. Amini, M. Marasi, T. Sritharan, M.J. Hadianfard, Mater. Chem. Phys. 118 (2009) 71-75.

[11] R. Amini, E. Salahinejad, M.J. Hadianfard, M. Marasi, T. Sritharan, Mater. Sci. Eng. A 527 (2010) 1135-1142.

[12] M.M. Cisneros, H.F. Lopez, H. Mancha, D. Vazquez, E. Valdes, G. Mendoza, M. Mendez, Metall. Mater. Trans. A 33 (2002) 2139-2144.

[13] M.M. Cisneros, H.F. Lopez, H. Mancha, E. Rincon, D. Vazquez, M.J. Perez, S.D.D.L. Torre, Metall. Mater. Trans. A 36 (2005) 1309-1316.

[14] M. Mendez, H. Mancha, M.M. Cisneros, G. Mendoza, J.I. Escalante, H.F. Lopez, Metall. Mater. Trans. A 33 (2002) 3273-3278.

[15] T. Haghir, M.H. Abbasi, M.A. Golozar, M. Panjepour, Mater. Sci. Eng. A 507 (2009) 144-148.

[16] D. Cui, X. Qu, P. Guo, K. Li, Powder. Metall. Technol. 26 (2008) 265-268.

[17] L. Guan, X. Qu, C. Jia, S. Wang, J. Univ. Sci. Technol. Beijing 27 (2005) 692-694.

[18] T. Fukutsuka, T. Anzai, M. Kaneda, Y. Matsuo, Y. Sugie, K. Fukaura, J. Soc. Mater. Sci. Jpn. 53 (2004) 1175-1179.

[19] L. Liu, L. Lu, L. Chen, Y. Qin, L.D. Zhang, Metall. Mater. Trans. A 30 (1999) 1097-1100.

[20] Y. Qin, L. Liu, L. Chen, J. Alloys Compd. 269 (1998) 238-240.

[21] E.P. Yelsukov, G.A. Dorofeev, A.V. Zagainov, N.F. Vildanova, A.N. Maratkanova, Mater. Sci. Eng. A 369 (2004) 16-22.

[22] F.A. Mohamed, Acta Mater. 51 (2003) 4107-4119.

[23] A. Inoue, T. Zhang, T. Masumoto, J. Non-Cryst. Solids 156–158 (1993) 473-480.

[24] A. Inoue, X.M. Wang, Acta Mater. 48 (2000) 1383-1395.

[25] E.S. Machlin, Thermodynamics and kinetics, Giro Press, New York, 1991.

[26] V.G. Gavriljuk, ISIJ Int 36 (1996) 738-745.

[27] E. Salahinejad, R. Amini, M. Marasi, M.J. Hadianfard, Mater. Des. 31 (2010) 527-532.

[28] E. Salahinejad, R. Amini, M. Marasi, M.J. Hadianfard, Mater. Des. 31 (2010) 2259-2263.

[29] E. Salahinejad, R. Amini, M.J. Hadianfard, Mater. Des. (2009), 31 (2010) 2241-2244.

**Figures:**

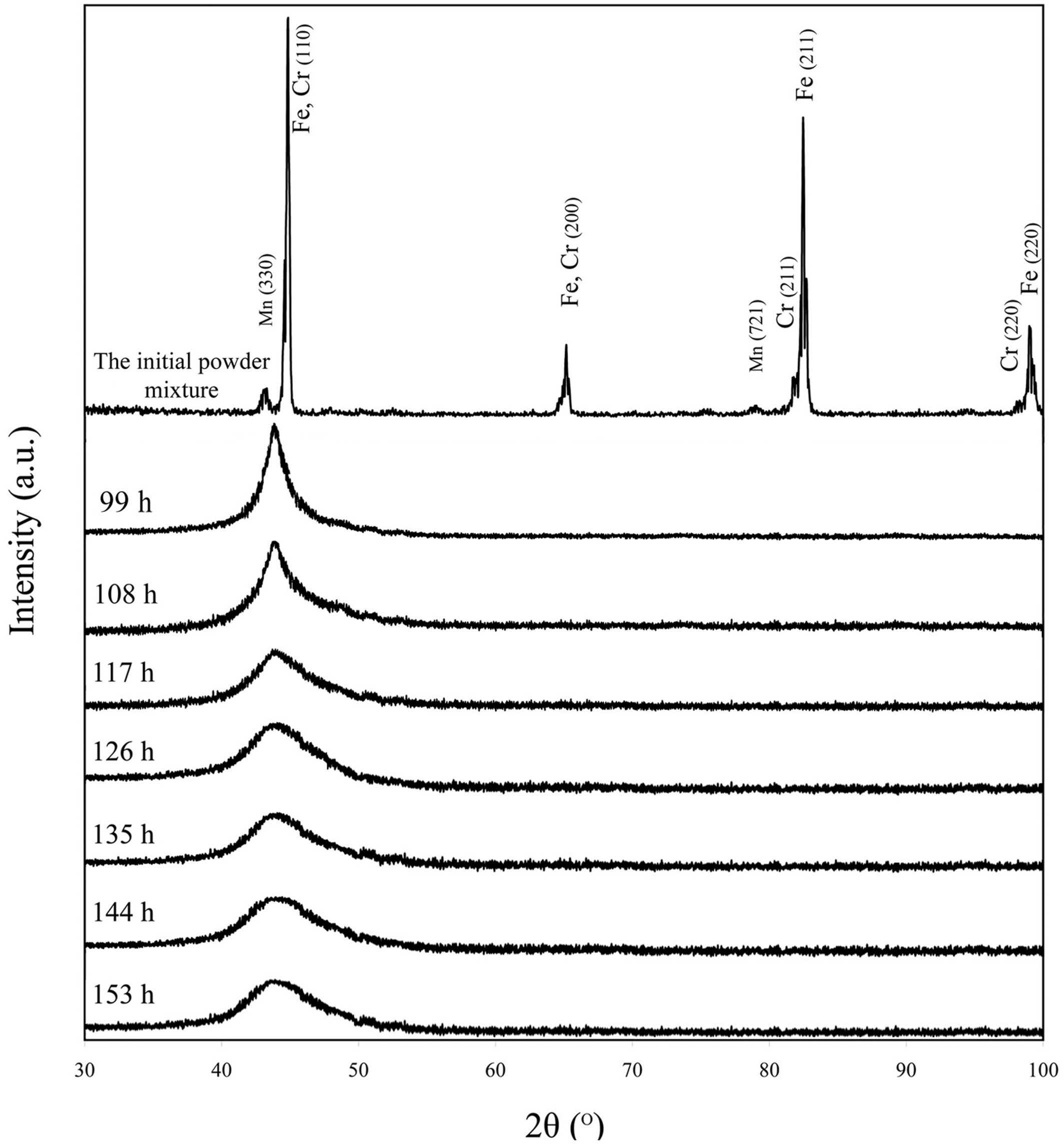

Fig. 1. XRD pattern of the initial powder mixture and the powders milled for 99, 108, 117, 126, 135, 144, and 153 h.

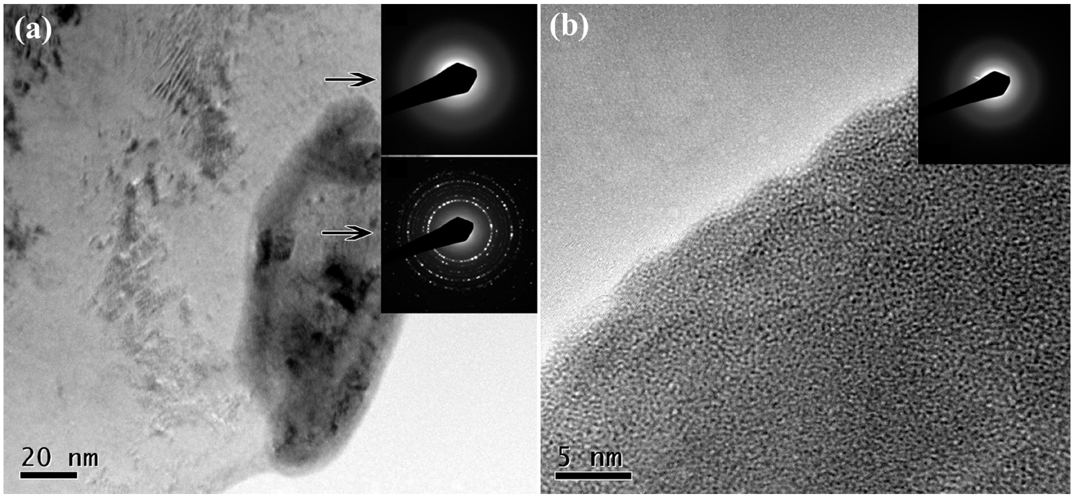

Fig. 2. TEM micrograph of the powders milled for (a) 117 and (b) 126 h. The inserts indicate the SAD pattern of the different regions.

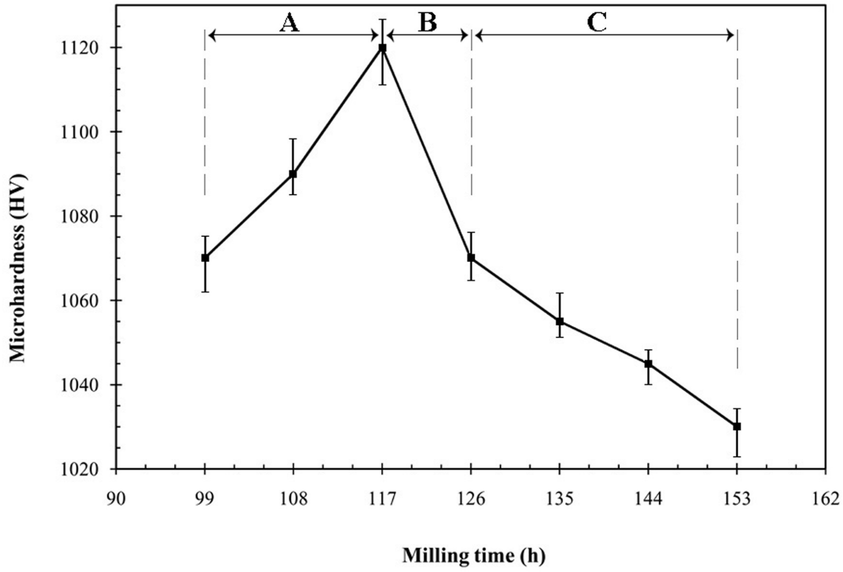

Fig. 3. Microhardness plot of the as-milled powder particles vs. the milling time.

E. Salahinejad, R. Amini, E. Askari Bajestani, M. Hadianfard, *Microstructural and hardness evolution of mechanically alloyed Fe–Cr–Mn–N powders*, Journal of alloys and compounds, 497 (2010) 369-372.
https://doi.org/10.1016/j.jallcom.2010.03.071

## Tables:

Table 1

Chemical composition of the as-milled powders (wt.%)

| Milling time (h) | Fe | Cr | Mn | N | O | C |
|---|---|---|---|---|---|---|
| 99 | 75.39 | 17.80 | 3.81 | 2.65 | 0.31 | 0.04 |
| 108 | 74.95 | 17.88 | 3.85 | 2.98 | 0.31 | 0.03 |
| 117 | 74.85 | 17.63 | 3.91 | 3.23 | 0.33 | 0.05 |
| 126 | 74.72 | 17.66 | 3.82 | 3.45 | 0.32 | 0.03 |
| 135 | 74.75 | 17.55 | 3.82 | 3.53 | 0.32 | 0.03 |
| 144 | 74.59 | 17.54 | 3.90 | 3.61 | 0.33 | 0.03 |
| 153 | 74.47 | 17.59 | 3.84 | 3.76 | 0.32 | 0.02 |

**This is the accepted manuscript (postprint) of the following article:**
E. Salahinejad, R. Amini, E. Askari Bajestani, M. Hadianfard, *Microstructural and hardness evolution of mechanically alloyed Fe–Cr–Mn–N powders*, Journal of alloys and compounds, 497 (2010) 369-372.
https://doi.org/10.1016/j.jallcom.2010.03.071

Table 2

Results of the XRD experiments on the as-milled powders, analyzed by the TOPAS software

| Milling time (h) | $\alpha$-phase percentage | $\gamma$-phase percentage | Amorphous percentage | $\alpha$-crystallite size (nm) | $\gamma$-crystallite size (nm) |
|---|---|---|---|---|---|
| 99 | 12.2 | 26.2 | 61.6 | 9.1 | 9.4 |
| 108 | 5.7 | 25.2 | 69.1 | 7.5 | 9.4 |
| 117 | 2.2 | 6.8 | 91 | 6.9 | 6.7 |
| 126 | - | - | 100 | - | - |
| 135 | - | - | 100 | - | - |
| 144 | - | - | 100 | - | - |
| 153 | - | - | 100 | - | - |